應用在無線通訊之低雜訊磷化銦鎵/砷化銦鎵假晶式高電子遷移率電晶體的高線性度之研究發展

研究生：張信源　　　　　　　　　　　　　指導教授：張翼博士

國立交通大學材料科學與工程學研究所

摘　　要

本篇論文主要目的在於發展應用於無線通訊之低雜訊磷化銦鎵/砷化銦鎵假晶式高電子遷移率電晶體之高線性度研究。

本次實驗在傳統矽平面摻雜元件結構的通道(channel layer)區域中加入微量的雜質濃度摻雜，使得電子在元件通道層中的分布更為均勻及對稱，以期望在不同的閘極偏壓條件下得到較為平坦的轉導值(Transconductance)分布曲線，改善磷化銦鎵/砷化銦鎵假晶式高電子遷移率電晶體的線性度表現。

同時，本研究另外於傳統矽平面摻雜元件結構的磷化銦鎵-蕭特基層(Schottky layer)中摻雜均勻的雜質濃度以改善元件線性度。此經由均勻摻雜後的磷化銦鎵層可以提升蕭特基接面的費米能階(Fermi level)準位，使元件的轉導值曲線分布(Transconductance)更為平坦，進而獲得較高的輸出三階交叉點功率(OIP3)。

經由等效電路分析理論及量測結果的驗證下，上述的元件結構設

計具有高三階交叉點功率，顯示出其在線性度上的表現獲得顯著的改善。此外，這兩個元件結構所具有的高三階交叉點功率對直流功率比值(IP3/P_{DC})同時顯示出其在低電壓-高線性度之無線通訊系統的應用上具有卓越的發展潛能。

Development of Low Noise InGaP/InGaAs PHEMTs with High Linearity for Wireless Communication Applications

Student：Xin-Yuan Chang **Advisor：Dr. Edward Y. Chang**

Department of Materials Science and Engineering

National Chiao Tung University

Abstract

The purpose of this dissertation is to develop the low noise InGaP/InGaAs PHEMTs with high linearity for wireless communications application.

A novel lightly-doped channel approach for linearity improvement of InGaP/InGaAs pseudomorphic high-electron-mobility transistor (PHEMT) device was presented. Light doping in the channel region of the conventional δ-doped InGaP/InGaAs PHEMT was adopted to provide a uniform and symmetric electron distribution in the channel region to achieve flat extrinsic transconductance (Gm) distribution under different gate bias conditions.

Another device structure with a uniformly-doped Schottky layer added to the conventional δ-doped InGaP/InGaAs PHEMT to improve device linearity was also studied it this dissertation. This added uniformly doped layer raises the Fermi level of the Schottky layer of the device which in turn contributes to a flatter extrinsic transconductance (Gm) profile,

resulting in higher third order intercept point (IP3).

The devices structure were determined based on the third-order intercept point (IP3) performance analysis through simple equivalent circuit model of the device, and the results showed substantial linearity improvement evidenced by much higher IP3. Furthermore, the very high IP3 to P_{DC} ratio of the devices developed will be of great potential for low-voltage high-linearity applications in wireless communications systems.

Acknowledgment

誌　　謝

能夠順利完成這份碩士論文，要感謝所有曾經幫助過我的師長、同學及朋友們。首先要對我的指導教授張翼博士表達深深的敬意。老師兩年來不只在課業上、實驗上給予許多指導與協助，同時在生活態度及為人處事觀念的養成上也有著深遠的影響，使我獲益良多。由衷感謝老師的諄諄教導。

其次，要感謝亦師亦友的林岳欽學長，在實驗上不厭其煩的給予我指導與協助，以及在日常生活上的關心，讓我在碩士生涯所學獲益匪淺，真的非常感謝你。

另外，要感謝許恆通博士、吳偉誠學長、黃珍嬅學妹在實驗量測上所給予的意見與幫助；感謝陳仕鴻、李晃銘、連亦中、褚立新、徐金鈺、黃瑞乾、呂宗育、張家源、郭建億、林龔樑等學長們在製程及儀器方面的協助及建議；感謝哲維、忠霖、志廷、柏舟、立翰、勃遠、鳥人、AAKING、SINGLE、NEGRO 及許許多多的同學們，有你們的陪伴，我的求學生涯更顯多彩多姿，謝謝你們。

最後，要特別感謝我的父母親、大哥、二哥、晨妤，在你們的全力支持與鼓勵下，才能使我在無後顧之憂下順利完成學業，真的非常感謝你們的照顧。

Contents

Abstract (in Chinese)

Abstract (in English)

Acknowledgement

Contents

Table Captions

Figure Captions

Chapter 1 Introduction 1

Chapter 2 Overviews of IM3 & IP3 5

2-1 One-tone input signal test 5

2-2 Two-tone input signal test 8

2-3 Analysis and Estimation of IM3 &IP3 10

Chapter 3 Experimental 15

3-1 Device structure 15

3-2 Device fabrication process 16

3-2.1 Wafer cleaning 17

3-2.2 Device isolation 17

3-2.3 Ohmic contact formation 29

3-2.4 Recess and gate formation 20

3-2.5 Device passivation 22

3-2.6 Nitride via etching 23

3-2.7 Air-bridge plating 24

Chapter 4 Characterization 26

4-1 DC Characteristics 26

4-1.1 ohmic contact resistance 26

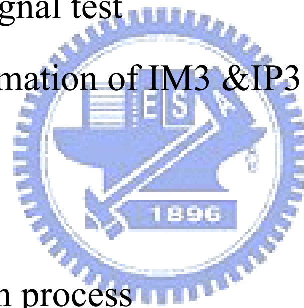

4-1.2 I_{ds}-V_{gs} polynomial curve fitting 28

4-1.3 extrinsic transconductance (G_m) 28

4-2 RF characteristics 29

4-2.1 Scattering parameters 29

4-3.2 Noise figure 30

4-3.3 Third-order intercept point (IP3) 31

Chapter 5 Results and Discussion 33

5-1 DC characteristics of the InGaP/InGaAs PHEMTs 33

5-1.1 Current-voltage curves (I-V curves) 33

5-1.2 extrinsic transconductance (G_m) 34

5-2 RF characteristics of the InGaP/InGaAs PHEMTs 35

5-2.1 Extraction of small-signal equivalent circuits 35

5-2.2 Noise figure 36

5-2.3 Third-order intercept point (IP3) 36

Chapter 6 Conclusions 38

References

Figures and Tables

Table Captions

Table 5.1 Comparisons of the DC characteristics of the three InGaP/InGaAs PHEMT devices.

Table 5.2 Extracted equivalent circuit parameters of the three devices for comparisons.

Table 5.3 Comparisons of the RF characteristics of the three InGaP/InGaAs PHEMT devices.

Figure Captions

Figure 1.1 Band-gap energy versus lattice constant diagram.

Figure 2.1 Illustration of the 1-dB Compression point.

Figure 2.2 Output power spectrum of the two-tone input signal.

Figure 2.3 Output fundamental power and third-order IMD power for an equal amplitude two-tone excitation.

Figure 2.4 A simple device equivalent circuit for linearity analysis.

Figure 3.1 Structure of the conventional delta doped InGaP/InGaAs PHEMT.

Figure 3.2 Structure of the delta doped InGaP/InGaAs PHEMT with lightly doped channel.

Figure 3.3 Structure of the delta doped InGaP/InGaAs PHEMT with uniform doping layer.

Figure 3.4 The band diagram of the InGaP/InGaAs PHEMT.

Figure 3.5 Process flow of the InGaP PHEMTs : (a) Mesa isolation and ohmic contact formation, and (b) gate recess and gate formation.(c) Device passivation and contact via formation, and (d) air-bridge plating.

Figure 3.6 The major steps of air-bridge formation.

Figure 3.7 The Image of the Finished 0.25x160 μm^2 InGaP/InGaAs PHEMT device.

Figure 4.1 The transmission line model (TLM) patterns.

Figure 4.2 Plot of measured resistance as a function of contact separation yields sheet resistance and contact resistance.

Figure 4.3 The equivalent two-port network schematic and the incident and reflected signals that occur.

Figure 4.4 PHEMT equivalent circuit with noise sources represented by voltage and current sources.

Figure 5.1 Ids-Vds curve of the conventional delta doped InGaP/InGaAs PHEMT.

Figure 5.2 Ids-Vds curve of the delta doped InGaP/InGaAs PHEMT with lightly doped channel.

Figure 5.3 Ids-Vds curve of the delta doped InGaP/InGaAs PHEMT with uniform doping layer.

Figure 5.4 Ids-Vgs curve of the three InGaP/InGaAs PHEMT devices at V_{ds} 1.5V.

Figure 5.5 g_m curve as a function of gate bias of the InGaP/InGaAs PHEMT devices at V_{ds} 1.5V.

Figure 5.6 PHEMT small-signal equivalent circuit model.

Figure 5.7 Measured *versus* modeled S-parameters for the conventional δ-doped InGaP/InGaAs PHEMT device. (a) S_{11} and S_{22} (b) S_{12} (c) S_{21}(Line: Measured, Line with marker: Modeled)

Figure 5.8 Measured *versus* modeled S-parameters for the lightly-doped channel InGaP/InGaAs PHEMT device. (a) S_{11} and S_{22} (b) S_{12} (c) S_{21}(Line: Measured, Line with marker: Modeled)

Figure 5.9 Measured *versus* modeled S-parameters for the uniformly-doped layer InGaP/InGaAs PHEMT device. S_{11} and S_{22} (b) S_{12} (c) S_{21} (Line: Measured, Line with marker: Modeled)

Figure 5.10 Noise figure of the InGaP/InGaAs PHEMT devices biased

at V_{ds} 1.5V and Ids = 20% Idss.

Figure 5.11 Measured OIP3 of the conventional delta doped InGaP/InGaAs PHEMT.

Figure 5.12 Measured OIP3 of the delta doped InGaP/InGaAs PHEMT with lightly doped channel.

Figure 5.13 Measured OIP3 of the delta doped InGaP/InGaAs PHEMT with uniform doping layer.

Figure 5.14 Measured IM3 levels *versus* power backed off from P_{1dB}.